Plant nanobionic materials with a giant temperature response mediated by pectin-Ca^{2+}

Raffaele Di Giacomo[a], Chiara Daraio[a,b,1], and Bruno Maresca[c]

[a]Department of Mechanical and Process Engineering, Swiss Federal Institute of Technology (ETH Zurich), 8092 Zurich, CH, Switzerland; [b]Division of Engineering and Applied Science, California Institute of Technology, Pasadena, CA 91125; and [c]Department of Pharmacy, Division of Biomedicine, University of Salerno, 84084 Fisciano, Italy

Edited by Michael S. Strano, Massachusetts Institute of Technology, Cambridge, MA, and accepted by the Editorial Board February 18, 2015 (received for review November 3, 2014)

Conventional approaches to create biomaterials rely on reverse engineering of biological structures, on biomimicking, and on bioinspiration. Plant nanobionics is a recent approach to engineer new materials combining plant organelles with synthetic nanoparticles to enhance, for example, photosynthesis. Biological structures often outperform man-made materials. For example, higher plants sense temperature changes with high responsivity. However, these properties do not persist after cell death. Here, we permanently stabilize the temperature response of isolated plant cells adding carbon nanotubes (CNTs). Interconnecting cells, we create materials with an effective temperature coefficient of electrical resistance (TCR) of −1,730% K^{-1}, ∼2 orders of magnitude higher than the best available sensors. This extreme temperature response is due to metal ions contained in the egg-box structure of the pectin backbone, lodged between cellulose microfibrils. The presence of a network of CNTs stabilizes the response of cells at high temperatures without decreasing the activation energy of the material. CNTs also increase the background conductivity, making these materials suitable elements for thermal and distance sensors.

temperature sensor | plant nanobionics | carbon nanotubes | iontronics | biomaterials

Materials that respond sensitively to temperature variations are used in several applications that range from electrical temperature sensors (1) to microbolometers for thermal cameras (2, 3). Existing high-performance temperature-sensitive materials, such as vanadium oxide, have temperature coefficient of electrical resistance (TCR) on the order of −6% K^{-1} at room temperature (4). These materials derive their properties from changes of their crystal structure during semiconductor to metal transitions (5). Higher sensitivities have been pursued by exploiting quantum effects (6–9), e.g., in carbon nanotube (CNT) composites (1). However, such composites reach lower TCRs because CNTs are embedded in an insulating polymeric matrix (1).

Variations of the ambient temperature influence the biopotential of living plants (10, 11). Experiments performed in vivo on a maple tree (*Acer saccharum*) showed an exponential correlation between the tree's branch electrical resistance and temperature (10). This behavior has been attributed to ionic conductivity occurring in plant cell walls (11). The plant cell wall has a highly complex macromolecular architecture with very dynamic structural and physiological properties (12). The cell wall, positioned outside the plasma membrane (13), is composed of carbohydrates such as cellulose microfibrils (14) with diameters as small as 3.0 nm (15) and hemicellulose interconnected with pectin. Pectins are composed of pectic polysaccharides rich in galacturonic acid that influence properties such as porosity, surface charge, pH, and ion balance and therefore are critical for ion transport within the cell wall. Pectins contain multiple negatively charged saccharides that bind cations, such as Ca^{2+}, that form cross-links that confer strength and expansibility to the cell wall (16–18). It has been shown that the gelation rate of pectin decreases exponentially with temperature so that the number of dissociated chains and free ions is higher at elevated temperatures (19). This finding was explained by an entropic effect: as the temperature increases, the probability of interaction between two pectin chains is reduced (19).

Biomaterials have been produced through different approaches, for example, reverse engineering of biological structures (20), biomimicking (21), and bioinspiration (22). To synthesize our materials, we invert these conventional approaches and allow biology to drive the fabrication. By culturing plant cells in the presence of CNTs, we obtain composite, multifunctional materials consisting of a biological matrix and synthetic nanoparticles. Biological cells–CNT composites have been fabricated earlier by combining multiwalled CNTs (MWCNTs) with plant or fungal cells (23, 24). These materials were shown to be electrically conductive and, in the case of BY-2 tobacco cells, have mechanical properties comparable to balsam fir wood (23). However, earlier studies of BY-2–MWCNT composites did not include their temperature response. Here, we describe the exceptionally high temperature- and moisture sensitivity of these materials and validate the mechanisms governing these responses.

Results and Discussion

Characterization. The microstructure of the produced material resembles that of natural wood (Fig. S1*A*). The presence of MWCNTs confers structural stability and a high electrical conductivity, which can be exploited to connect the samples to an external circuit. Hence, we termed the material cyberwood. The method used to synthesize this material is very inexpensive and scalable. We produced and tested two sets of samples at different scales varying in volume by ∼4 orders of magnitude (*Materials and Methods*). We demonstrate the use of these materials as scalable thermal sensors and describe the fundamental mechanisms governing their response.

Significance

We present a bionic material made of plant cells and carbon nanotubes (CNTs) that exhibits record high temperature sensitivity. This material outperforms by ∼2 orders of magnitude the best man-made materials. The basic mechanism governing this response is the ionic conductivity in the egg-box structure of the pectin backbone, which interconnects cellulose microfibrils in the plant cell wall. The use of CNTs allows the bioelectrical property found in living plants to persist after cell death and stabilizes the response of the dried cells at high temperatures.

Author contributions: R.D.G., C.D., and B.M. designed research; R.D.G. performed research; R.D.G., C.D., and B.M. analyzed data; and R.D.G., C.D., and B.M. wrote the paper.

The authors declare no conflict of interest.

This article is a PNAS Direct Submission. M.S.S. is a guest editor invited by the Editorial Board.

[1]To whom correspondence should be addressed. Email: daraio@ethz.ch.

This article contains supporting information online at www.pnas.org/lookup/suppl/doi:10.1073/pnas.1421020112/-/DCSupplemental.

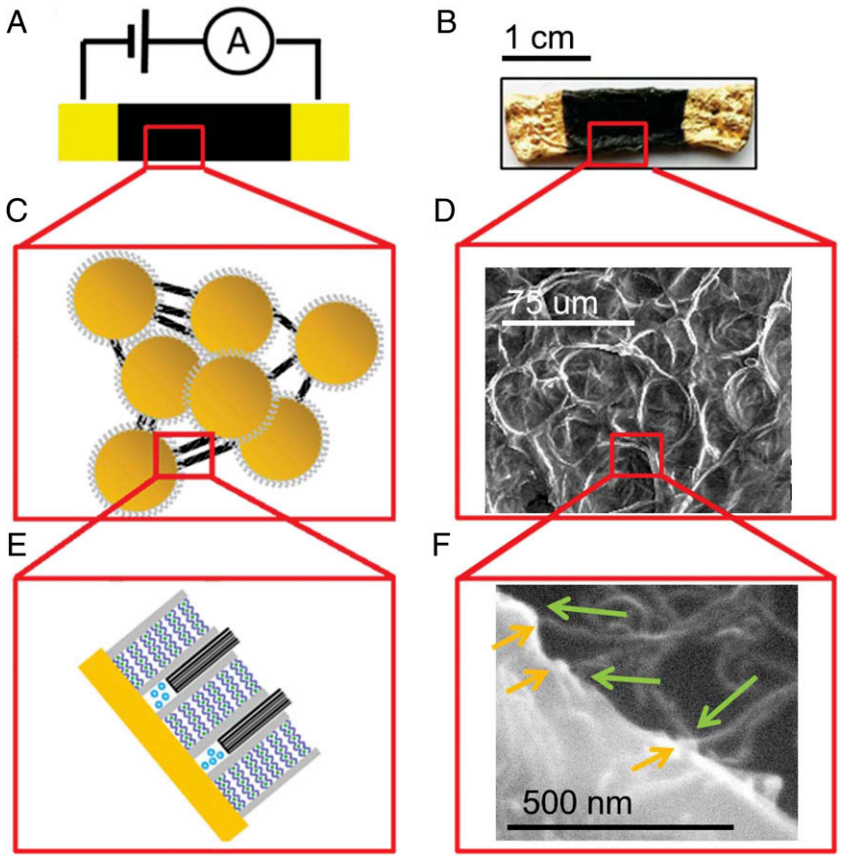

Fig. 1. Schematic diagrams and scanning electron microscopy (SEM) images of cyberwood. (*A*) Representation of the material (black) with sputtered coplanar gold electrodes (yellow) and current measurement setup. (*B*) Optical image of a sample. (*C*) Diagram of BY-2 cells (gold) with MWCNTs (black lines). The cell walls are emphasized in gray. (*D*) SEM picture of tobacco cell (dark gray) with MWCNTs inside the cell wall (brighter lines). (*E*) Schematic diagram of the pectin backbone structure (blue lines) interconnecting cellulose microfibrils (gray bars), and the encapsulated metal ions (green circles) in the egg-box structure. Micropores between cellulose microfibrils are shown filled with water (light blue circles) and/or MWCNTs. (*F*) SEM image showing MWCNTs penetrating the cell wall of a BY-2 cell. Orange arrows indicate the edge of the cell wall and green arrows indicate the MWCNTs.

To measure the electrical properties of the larger (macroscale) samples we sputtered coplanar gold electrodes at their extremities (Fig. 1 *A* and *B*), and to measure the smaller (microscale) samples we deposited them on gold electrodes on a substrate. We also performed measurements with steel contacts and we found no significant difference. Scanning electron microscopy images of the samples show that MWCNTs partially penetrate the cell wall and form a complex network among cells (Fig. 1 *C* and *D*). A schematic diagram of the MWCNTs–cell wall nanostructure, comprising the pectin backbone (25), is shown in Fig. 1*E*. For a discussion and references about the model in Fig. 1*E*, see *SI Text*, *CNT and Cell Wall Penetration* and Fig. S1*B*.

Resistance of the larger samples was monitored as a function of temperature at different values of moisture content, following different thermal cycles (Fig. 2*A*). Samples were subjected to slow temperature variations, between 35 °C and 75 °C, to control the sample's moisture content. All measurements, performed at thermal equilibrium, showed that resistance decreased with increasing temperature. The measured resistance decreased by almost 3 orders of magnitude in a 40 °C temperature increase. This value corresponds to an effective TCR of $-1{,}730\%\ K^{-1}$ (Table S1). To determine the stability of the material over a long period, we measured the variation of the current as a function of time at constant temperature (Fig. 2*B*). In these tests we rapidly ramped the temperature of samples with different moisture contents from 35 °C to 75 °C and held the temperature constant at 75 °C for approximately 100 min before cooling. Samples with increasingly higher moisture content showed a decrease of the measured current at constant temperature, indicating they were drying. Because the sample measured at 75 °C at 0% moisture (magenta curve) showed no change in the current with time, we assumed that it could not have been dried further at this temperature (see also additional experiments reported in Fig. S2*A* and its discussion). The process of dehydration is reversible (Fig. S2*B*).

To quantify the effect of the moisture content on the sample's electrical response, we measured the variation of the sample's electrical resistance as a function of the sample's weight (indicating different water content; Fig. 2*C*). The colored circles around each experimental point in Fig. 2*C* correspond to the colors in Fig. 2 *A* and *B*. These results suggest that cyberwood can be used as a humidity sensor as long as temperature is kept constant. The same material can be used as a temperature sensor as long as humidity is kept constant. To show that it is possible to discriminate between the temperature contribution and that of the moisture of the environment, without monitoring the sample's weight, we encased the material in a polymeric housing (Fig. S3). The presence of the housing did not change the measured temperature response (Fig. S3, *Inset*).

The optimal performance of cyberwood was found below 100 °C. Above this temperature, the properties of the cellular material decrease. To identify the maximum operating temperature of the material, we measured the electrical resistance cycling the samples at increasing temperatures up to 200 °C (Fig. 2*D*). Measurements revealed an unchanged sensitivity from 25 ° up to

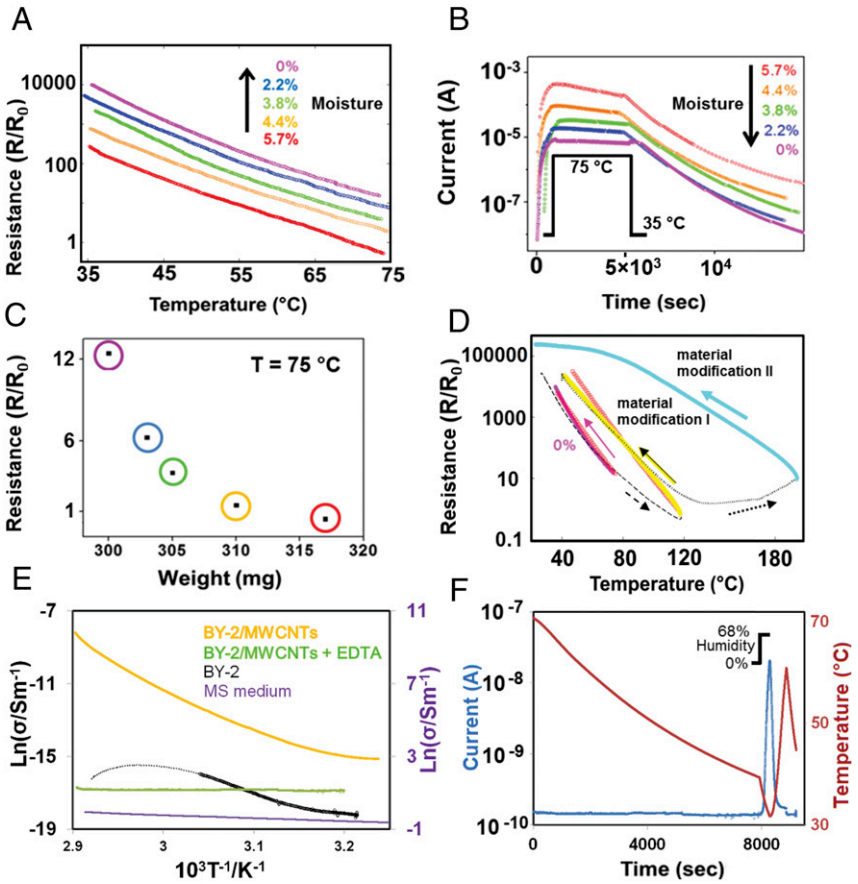

Fig. 2. Response of cyberwood to temperature and moisture content variations. (*A*) Electrical resistance vs. temperature at different moisture contents: 5.7% (red), 4.4% (yellow), 3.8% (green), 2.2% (blue), 0% (magenta). Red squares represent numerical simulations. (*B*) Current vs. time during temperature cycles. Cycle I: 5.7% moisture content (red), cycle II: 4.4% moisture content (yellow), cycle III: 3.8% moisture content (green), cycle IV: 2.2% moisture content (blue), cycle V: 0% moisture content (magenta). (*C*) Resistance vs. sample's weight at 75 °C. The weight loss corresponds to the moisture content: 5.7% (red), 4.4% (yellow), 3.8% (green), 2.2% (blue), 0% (magenta). (*D*) Electrical resistance vs. temperature during cycles up to 200 °C. Magenta line: same measurement as in *A* at 0% moisture. The dashed line and arrow represent the sample cycling up to 120 °C. Yellow line: cycle from 120 °C to 40 °C. Dotted line: cycles up to 200 °C. Cyan line: cycle from 200 °C to 23 °C. The open squares represent the response measured up to 75 °C. The arrows indicate whether the measurement was performed during the heating or cooling part of the respective cycles. (*E*) Arrhenius plot of the conductivity of a cyberwood microsample (yellow line); isolated BY-2 tobacco cells (black line values over 55 °C are dotted); cyberwood microsample with addition of EDTA (green line) and MS medium (purple line). (*F*) Temperature vs. time (red line) and current vs. time (blue line) in a cyberwood microsample with addition of EDTA. The ambient relative humidity was suddenly increased at time t = 8,000 s.

approximately 100 °C, above which irreversible modifications of the cellular matrix occurred. When the sample was heated to 120 °C (dotted line) and then slowly cooled to 40 °C (yellow line) its color changed from black to brown, which suggests that structural changes had occurred. To emphasize the change in slope of the curves we drew two parallel lines (red squares) representing the response measured up to 75 °C. When the sample was heated to 200 °C the material changed further its electrical temperature behavior. This was expected because, in simulations reported earlier, cellulose changes its molecular structure at similar temperatures (26). During this higher temperature cycle the sample's color changed to dark woody-brown tone and its weight reduced considerably and irreversibly. Nevertheless, the resistance–temperature response spanned almost 4 orders of magnitude (cyan line in Fig. 2*D*).

Sensing Mechanisms. We performed experiments to understand the mechanisms contributing to the extreme temperature and humidity sensitivity of the cyberwood. We expected mixed ionic and electronic conductivities and designed tests to deconvolve the contribution of each mode. Fig. 2*E* shows the Arrhenius plots of the conductivity of a cyberwood microsample (BY-2–MWCNTs, yellow line) and that of control experiments. We found no variation in the microsample temperature response compared with larger samples. Measurements on samples obtained with isolated tobacco cells in the absence of MWCNTs (BY-2, black line) also presented high temperature responsivity, although this phenomenon was transient. Because BY-2 samples required high water content for being conductive, they became unstable at temperatures above 55 °C (black dotted line) due to water loss. In addition, even at low temperatures, their lifetime was limited to a few cycles, due to cell death and loss of structural stability. Cyberwood samples tested over a 12-mo period did not show any change in their thermal or mechanical response. These experiments proved that the cyberwood's sensitivity to temperature is primarily due to the structure of plant cells.

The temperature sensitivity of plants is due to the presence of ions in the cell wall (11). The egg-box structure of pectin inside the plant's cell wall contains metal ions such as Ca^{2+} (25); Fig. 1*E*. These ions are responsible for the cross-linking between pectin chains, and this process is disfavored as temperature increases (19). As a consequence, the number of free ions available for conduction increases with temperatures. To investigate the role of Ca^{2+} ions, we measured microsamples

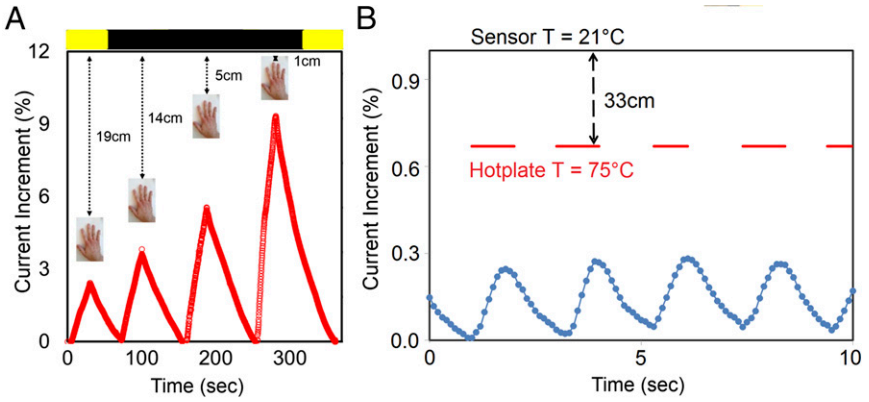

Fig. 3. Cyberwood as a thermal distance sensor. Plots show variations of the current in different cyberwood samples, as a function of the position, in- and off-axis, of heat-emitting bodies in time. (*A*) Larger sample detecting the position of a hand. (*B*) Microsample detecting the position of a hotplate.

treated with 15 μL of 0.5 M EDTA, a chelating agent for divalent ions (Fig. 2*E*, green line). The addition of EDTA eliminated the temperature sensitivity of the material proving the central role of pectin-Ca^{2+}. The conductance increment due to the presence of MWCNTs is constant in temperature (Fig. 2*E*; compare black and yellow lines), whereas the number of free Ca^{2+} ions available for current transport increases exponentially with temperature. The presence of MWCNTs provides a permanent conductive pathway, and substitutes water when the material is completely dehydrated. Therefore, MWCNTs are responsible for raising the background conductivity and stabilizing the electrical response, whereas the number of Ca^{2+} available for conduction is responsible for the current increase with temperature.

The sample's sensitivity to humidity was still present after adding EDTA (Fig. 2*F*). For the results reported in Fig. 2*F*, the sample was tested at low, constant relative humidity while changing the temperature (monitored with an independent thermometer). After ∼2 h (∼8,000 s) the humidity of the environment was suddenly increased to 68% and subsequently decreased. The measured current increased sharply and then decreased, following humidity, and independently of the temperature. This demonstrates that the sensitivity of cyberwood to humidity is not related to the presence of divalent Ca^{2+} ions and can be decoupled from the temperature response.

The cyberwood's conductivity increases ∼25 times when the internal moisture content is increased between 0% and 5.7% at 75 °C. A comparable behavior has been described for microcrystalline cellulose (MCC) and has been attributed to protons jumping between neighboring water molecules bound to cellulose OH^- groups on the amorphous microfibril surfaces (27–29). Cyberwood presents similar density (1.03 g/cm^3) to MCC (27–29). In addition, the cyberwood fractal dimension, measured using impedance spectroscopy (23), is D = 2.4 and is in line with values reported for MCC in ref. 27. The concomitant presence of these two parameters indicates the presence of micropores, which have dimensions between 5 and 35 nm. The magnitude of the water-induced proton conductivity, at given moisture content, is determined by the connectivity of the micropores (29). At densities between ∼0.7 and 1.2 g/cm^3 the pore networks were shown to percolate, facilitating the charge transport through the MCC compact (29). The same mechanism is supposed to occur in cyberwood.

To compare the cyberwood's response with that of an electrolyte with the same ionic strength as that present in plant cells, we tested the temperature sensitivity of Murashige and Skoog (MS) growth medium only, as shown in Fig. 2*E* (purple line). It is evident that the TCR of the MS medium is rather small. Temperature response of cyberwood is also ∼300 times higher than the best electrolyte materials, either solid, liquid, gel, organic, or polymeric (30).

Temperature at Distance. The very high responsivity to temperature changes of cyberwood suggests that it can be used as a temperature distance sensor. The distance of a warm body from the sensor can be inferred from temperature measurements performed at constant environmental conditions (Fig. S4). Fig. 3 shows the capacity to detect the presence of bodies irradiating heat (e.g., a hand and a hotplate) positioned at different distances from the sensor. We tested two cyberwood samples (a larger one and a smaller one) placed in an open oven at 23 °C, at constant relative humidity. We first measured the variation of current across the larger sample in response to the motion of a hand positioned in four different locations, ranging from 1 to 19 cm away from the sample (Fig. 3*A*). At each position, the hand was held still for 30 s and then rapidly moved away. In correspondence to each hand movement, the current measured across the sample ramped to a different value and then decreased to a reference value corresponding to a temperature of 23 °C. A similar experiment was performed to detect the motion of an adult moving in a room (Fig. S4). We then measured the response of the smaller sample to movements in- and off-axis of a hotplate held at constant temperature, located 33 cm away from the sample (Fig. 3*B*). The smaller sample was also sensitive to variations in the position of the hotplate.

Cyberwood is an example of how plant nanobionics (31) can be exploited to create materials with record high temperature sensitivity.

Materials and Methods

We prepared a 1% SDS solution in MilliQ water and added MWCNTs. We let the solution rest for 150 min. To reduce the clusters in the solution we then sonicated the suspension at room temperature for 20 min. Following, we performed additional purification steps: After sonication, the supernatant was collected and allowed to precipitate for 18 h in a new container. The supernatant was collected again, centrifuged at 10,000 rpm for 5 min at room temperature, and the final supernatant was used for experiments. This solution was added to a suspension of growing tobacco BY-2 cells (23). Five independent cells–MWCNTs samples were produced and each analyzed individually. Commercially available CNTs (nonmodified type 3100 MWCNTs, Nanocyl) were used in the solution with SDS. The BY-2 cell line was derived from the callus of seedlings of *Nicotiana tabacum* and propagated in modified MS medium supplemented with 3% sucrose, 600 μg/mL KH_2PO_4, 0.2 μg/mL 2,4-dichlorophenoxacetic acid, and 30 μg/mL thiamine-HCl. Cells were grown in large flasks on a rotary shaker at 130 rpm at 25 °C in the dark. Ten percent of stationary phase cells was transferred to a fresh medium every week. Spontaneous aggregation of cells was observed with tobacco cells combined with MWCNTs. After 24 h a gel-like material formed, was collected and dried at 47 °C for 15 d. We fabricated macroscopic samples ∼2 cm long, ∼1 cm wide, and ∼3 mm thick, and microscopic samples 500 μm

long, 3 mm wide, and 50 μm thick. Control samples of BY-2 only cells were produced depositing and compacting a single layer of BY-2 cells on a substrate. The control samples had the same dimensions as the microscopic samples. See *SI Materials and Methods* for details on the measurements, setups, and characterization.

ACKNOWLEDGMENTS. The authors thank Karsten Kunze from the Scientific Center for Optical and Electron Microscopy (ScopeM) of the Eidgenössiche Technische Hochschule Zürich, and R. Thevamaran for support with SEM imaging. This work was supported by Swiss National Science Foundation Grant SNF 157162.

1. Alamusi, et al. (2013) Temperature-dependent piezoresistivity in an MWCNT/epoxy nanocomposite temperature sensor with ultrahigh performance. *Nanotechnology* 24(45):455501.
2. Syllaios AJ, et al. (2000) Amorphous silicon microbolometer technology. *MRS Proc* 609(A14):4.
3. Vollmer M, Möllmann K-P (2010) *Infrared Thermal Imaging: Fundamentals, Research and Applications* (John Wiley & Sons, Hoboken, NJ).
4. Wang B, Lai J, Li H, Hu H, Chen S (2013) Nanostructured vanadium oxide thin film with high TCR at room temperature for microbolometer. *Infrared Phys Technol* 57:8–13.
5. Narayan J, Bhosle VM (2006) Phase transition and critical issues in structure-property correlations of vanadium oxide. *J Appl Phys* 100:103524.
6. Li C, Thostenson ET, Chou T-W (2007) Dominant role of tunneling resistance in the electrical conductivity of carbon nanotube–based composites. *Appl Phys Lett* 91: 223114.
7. Bockrath M, et al. (1999) Luttinger-liquid behavior in carbon nanotubes. *Nature* 397:598–601.
8. Sheng P (1980) Fluctuation-induced tunneling conduction in disordered materials. *Phys Rev B* 21(6):2180.
9. Simmons JG (1963) Generalized formula for the electric tunnel effect between similar electrodes separated by a thin insulating film. *J Appl Phys* 34:1793.
10. Fensom DS (1960) A note on electrical resistance measurements in *Acer saccharum*. *Can J Bot* 38(2):263–265.
11. Fensom DS (1966) On measuring electrical resistance in situ in higher plants. *Can J Plant Sci* 46(2):169–175.
12. Caffall KH, Mohnen D (2009) The structure, function, and biosynthesis of plant cell wall pectic polysaccharides. *Carbohydr Res* 344(14):1879–1900.
13. Cifuentes C, Bulone V, Emons AMC (2010) Biosynthesis of callose and cellulose by detergent extracts of tobacco cell membranes and quantification of the polymers synthesized in vitro. *J Integr Plant Biol* 52(2):221–233.
14. Fernandes AN, et al. (2011) Nanostructure of cellulose microfibrils in spruce wood. *Proc Natl Acad Sci USA* 108(47):E1195–E1203.
15. Thomas LH, et al. (2013) Structure of cellulose microfibrils in primary cell walls from collenchyma. *Plant Physiol* 161(1):465–476.
16. Van Buren JP (1991) Function of pectin in plant tissue structure and firmness. *The Chemistry and Technology of Pectin*, eds Walter RH, Taylor S (Academic, San Diego), pp 1–22.
17. Peaucelle A, Braybrook S, Höfte H (2012) Cell wall mechanics and growth control in plants: The role of pectins revisited. *Front Plant Sci* 3:121.
18. Hu H, Brown PH (1994) Localization of boron in cell walls of squash and tobacco and its association with pectin evidence for a structural role of boron in the cell wall. *Plant Physiol* 105(2):681–689.
19. Cardoso SM, Coimbra MA, Lopes da Silva JA (2003) Temperature dependence of the formation and melting of pectin–Ca2+ networks: A rheological study. *Food Hydrocoll* 17(6):801–807.
20. Nawroth JC, et al. (2012) A tissue-engineered jellyfish with biomimetic propulsion. *Nat Biotechnol* 30(8):792–797.
21. Guerette PA, et al. (2013) Accelerating the design of biomimetic materials by integrating RNA-seq with proteomics and materials science. *Nat Biotechnol* 31(10): 908–915.
22. Leslie DC, et al. (2014) A bioinspired omniphobic surface coating on medical devices prevents thrombosis and biofouling. *Nat Biotechnol* 32(11):1134–1140.
23. Di Giacomo R, et al. (2013) Bio-nano-composite materials constructed with single cells and carbon nanotubes: Mechanical, electrical, and optical properties. *IEEE Trans NanoTechnol* 12(6):1026–1030.
24. Di Giacomo R, et al. (2013) *Candida albicans*/MWCNTs: A stable conductive bio-nanocomposite and its temperature sensing properties. *IEEE Trans NanoTechnol* 12(2): 111–114.
25. Sriamornsak P (2003) Chemistry of pectin and its pharmaceutical uses: A review. *Silpakorn Univ Int J* 3:206–228.
26. Matthews JF, et al. (2011) High-temperature behavior of cellulose I. *J Phys Chem B* 115(10):2155–2166.
27. Nilsson M, Mihranyan A, Valizadeh S, Strømme M (2006) Mesopore structure of microcrystalline cellulose tablets characterized by nitrogen adsorption and SEM: The influence on water-induced ionic conduction. *J Phys Chem B* 110(32):15776–15781.
28. Nilsson M, Alderborn G, Strømme M (2003) Water-induced charge transport in tablets of microcrystalline cellulose of varying density: Dielectric spectroscopy and transient current measurements. *Chem Phys* 295(2):159–165.
29. Nilsson M, Frenning G, Gråsjö J, Alderborn G, Strømme M (2006) Conductivity percolation in loosely compacted microcrystalline cellulose: An in situ study by dielectric spectroscopy during densification. *J Phys Chem B* 110(41):20502–20506.
30. Kamaya N, et al. (2011) A lithium superionic conductor. *Nat Mater* 10(9):682–686.
31. Giraldo JP, et al. (2014) Plant nanobionics approach to augment photosynthesis and biochemical sensing. *Nat Mater* 13(4):400–408.